Available online at www.sciencedirect.com
ScienceDirect
Journal of Sound and Vibration 301 (2007) 278–296
JOURNAL OF SOUND AND VIBRATION
www.elsevier.com/locate/jsvi

Acoustic measurement of boundary layer flow parameters

M.G. Smith[a,*], S. Whale[b]

[a]Institute of Sound and Vibration Research, University of Southampton, Southampton SO17 1BJ, UK
[b]Gill Electronics R&D, Lymington SO41 9EG, UK

Received 20 October 2005; received in revised form 30 August 2006; accepted 9 October 2006
Available online 15 December 2006

Abstract

The principle of an ultrasonic method for measuring the parameters of a boundary layer flow is investigated using a mathematical model of the sound field created by a compact piston in a solid boundary, radiating into a parallel shear flow. The model, based on a wavenumber decomposition of the problem, is used to demonstrate that dispersive effects in the streamwise direction are a function of the free-stream flow velocity and the boundary layer displacement thickness, and that a multifrequency measurement of phase velocity between two wall-mounted transducers can in principle be used to determine these parameters. Results from a preliminary experiment to demonstrate the method are presented.

1. Introduction

Ultrasonic techniques for measuring flow speed based on a measurement of the convected speed of sound are well established for situations where uniform flow may be assumed over the propagation path, e.g. for fluid flowing in a duct where the measurement is made using the plane wave acoustic mode [1], or for anemometry in the atmosphere [2]. In these cases, sound propagation is non-dispersive and the time of flight of a pulse of sound as it travels from a source transducer to a receiver transducer may be measured unambiguously. Here, we consider a different application, where it is required to measure the free-stream velocity and boundary layer thickness non-invasively for steady flow over a flat boundary. The principle of the method considered here specifically exploits the dispersive behaviour of sound propagating in the non-uniform flow so as to determine the properties of the boundary layer.

A flow-measuring device based on this principle would comprise a source and one or more receiver transducers, flush mounted in the surface, with an electronic system for measuring phase velocity between source and each receiver. By measuring over a distance that is large compared with the thickness of the boundary layer the effect of unsteadiness in the boundary layer flow is averaged out to provide a measurement of the mean parameters.

Some preliminary measurements using a prototype system are described in Section 5 of this paper. Such a system could be useful in determining the characteristics and state of the flow over the wings or fuselage of an

*Corresponding author.
E-mail address: mgs@isvr.soton.ac.uk (M.G. Smith).

0022-460X/$ - see front matter © 2006 Elsevier Ltd. All rights reserved.
doi:10.1016/j.jsv.2006.10.007

aircraft, the hull of a ship or sails of a boat, the aerodynamic surfaces of racing cars, etc., and may be useful for model scale wind tunnel testing or on full-scale vehicles.

2. Problem outline

The problem of interest for a mathematical model of the measurement device is shown in Fig. 1. A two-dimensional (2D) line or three-dimensional (3D) point source radiates sound into a parallel shear flow, comprising an idealised boundary layer which separates a solid surface at $z = 0$ from a region of uniform flow in the region $\delta < z < \infty$. The model needs to predict the acoustic pressure distribution over the wall, including the phase change between source and receiver, but does not necessarily need to predict the sound field in the body of the fluid. The undisturbed flow is assumed to have the form $\mathbf{U} = (U(z), 0, 0)$; thus it flows in the x-direction and is uniform in any plane $z =$ constant.

Given this assumed flow, the problem is homogeneous in the time and space variables t, x, and y, and the governing equations, which are described in Appendix, may be solved in the Fourier transformed frequency/wavenumber domain using variables ω, k_x and k_y. Using acoustic pressure p as an example, the convention used for the transform is that solutions of the following form are sought:

$$p(x, y, z, t) = \tilde{p}(k_x, k_y, z)\mathrm{e}^{\mathrm{j}(\omega t - k_x x - k_y y)}. \tag{1}$$

Here, $\tilde{p}(k_x, k_y, z)$ is the pressure field generated at height z by the wall vibration at angular frequency ω and wavenumber components k_x, k_y. The $\sim$ is used above to denote a transformed variable, but from now on this will be dropped for clarity.

If, for frequency ω, a solution for $p(k_x, k_y, z)$ is known for all wavenumbers, then the radiated pressure in the spatial domain may be obtained from the inverse Fourier transform:

$$p(x, y, z) = \frac{1}{(2\pi)^2}\iint p(k_x, k_y, z)\mathrm{e}^{-\mathrm{j}(k_x x + k_y y)}\,\mathrm{d}k_x\,\mathrm{d}k_y. \tag{2}$$

The solution is driven by the spatial wall velocity distribution for the source piston in the rigid wall, $u_w(x, y)$, which may be Fourier transformed to give wall vibration as a function of wavenumber:

$$u_w(k_x, k_y) = \iint u_w(x, y)\mathrm{e}^{\mathrm{j}(k_x x + k_y y)}\,\mathrm{d}x\,\mathrm{d}y. \tag{3}$$

For a point source located on the wall at (x_0, y_0), as used in later sections, the wavenumber spectrum is flat. It is chosen as $u_w(k_x, k_y) = \mathrm{e}^{\mathrm{j}(k_x x_0 + \mathrm{j}k_y y_0)}$, so that $|u_w| = 1$ for all k_x and k_y.

At the wall, $z = 0$, the acoustic pressure and the wall velocity at each wavenumber are related via the radiation impedance of the wall, $Z_{\mathrm{rad}}(k_x, k_y)$:

$$p(k_x, k_y, 0) = Z_{\mathrm{rad}}(k_x, k_y)u_w(k_x, k_y). \tag{4}$$

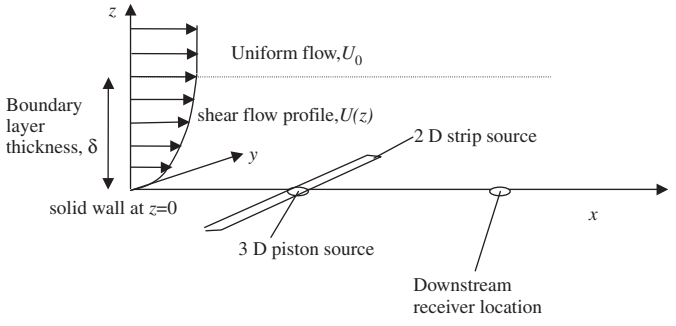

Fig. 1. Outline of the measurement system and the model. A source mounted in the wall at $z = 0$ radiates sound into a parallel shear flow representing a boundary layer, and the sound field is measured downstream by a receiver mounted in the wall. Either 2D or 3D or models may be appropriate.

Substituting (4) into (2), the spatial pressure field at the wall is thus given by

$$p(x,y,0)=\frac{1}{(2\pi)^2}\iint Z_{\mathrm{rad}}(k_x,k_y)u_w(k_x,k_y)\mathrm{e}^{\mathrm{j}(k_x x+k_y y)}\,\mathrm{d}k_x\,\mathrm{d}k_y. \tag{5}$$

Eq. (5) applies to 3D problems. For a 2D problem k_y is set to zero in (5) and only a single Fourier integral is performed.

A method for evaluating the radiation impedance of a vibrating surface radiating into a parallel shear flow is given in Refs. [3,4]; the governing differential equations for the propagation of an outgoing wave have to be solved, starting from a radiation condition into the region of uniform flow. These references, however, deal not only with the radiation impedance of the surface, but also with the sound field created in the body of the fluid. As already noted, this is not required for the flow measurement problem because both source and receiver are assumed to lie at the boundary, and so the mathematical model may be simplified as described in Appendix to this paper.

To evaluate Eq. (5) the radiation impedance is required for all wavenumber components. In principle this covers an infinite range of wavenumbers, and in practice it is necessary both to truncate the integration beyond a certain wavenumber range and to evaluate the integrand at only a finite number of wavenumbers.

3. Characteristics of the radiation impedance and the sound pressure field at the wall

In this section numerical results are presented to illustrate the effects of flow, first on the radiation impedance (Section 3.1) and then on the spatial characteristics of the modulus of the pressure field around a 2D line source (Section 3.2) and a 3D point source (Section 3.3). The phase information in the sound field, which is used for flow measurement, is considered in Section 4.

3.1. Radiation impedance

The effect of the shear flow on the source is to modify the radiation impedance $Z_{\mathrm{rad}}(k_x, k_y)$ and hence the radiated pressure field. Fig. 2 shows, for a Mach 0.6 flow and with $k_y = 0$, the radiation impedance as a function of k_x/k for four different non-dimensional boundary layer thicknesses δ/λ, where k is the acoustic wavenumber ω/c_0, λ is the acoustic wavelength and c_0 is the local speed of sound. For a thin boundary layer, with $\delta/\lambda = 0.01$, the radiation impedance is close to the uniform flow solution ($\delta/\lambda = 0$) given by Morse and Ingard [6], with peaks in the real part of the radiation impedance close to $(k_x/k) = (\pm 1/(1 \pm M_0))$ where the propagation speed of the waves in the surface is sonic relative to the free-stream flow. Outside of this wavenumber range the radiation impedance is purely imaginary because waves are cut-off in the free-stream flow and no power is radiated away from the surface [3]. For thicker boundary layers the real part of the radiation impedance at negative wavenumbers is reduced compared with the thin boundary layer solution because these waves have to tunnel through the low-speed flow near the surface [4]. The imaginary part of the radiation impedance shows peaks at wavenumbers where channelled 'modes' occur in the boundary layer. These large positive wavenumbers propagate subsonically relative to the flow, and the radiated acoustic pressure wave decays exponentially away from the surface so that they do not contribute significantly to the pressure field away from the surface; nonetheless they must be included for the purposes of predicting the pressure at the surface, especially near the source.

3.2. Pressure field at the wall for a 2D line source

Having determined the radiation impedance for each wavenumber, Eq. (5) may be used to determine the pressure field at the wall. As previously noted, for 2D solutions k_y is set to zero and only a single Fourier integral is performed. For computational reasons it is necessary to limit the integration to a finite wavenumber range, and to approximate the continuous Fourier transform by a discrete fourier transform (DFT), so that the integrand only has to be evaluated at a finite number of wavenumber values. For each of the 2D solutions presented in the following sections an 8192 point transform was used, with a wavenumber range of $-3 < k_x/k < 3$ at low Mach numbers ($M_0 \leqslant 0.3$) or $-6 < k_x/k < 6$ at higher Mach numbers. The wavenumber

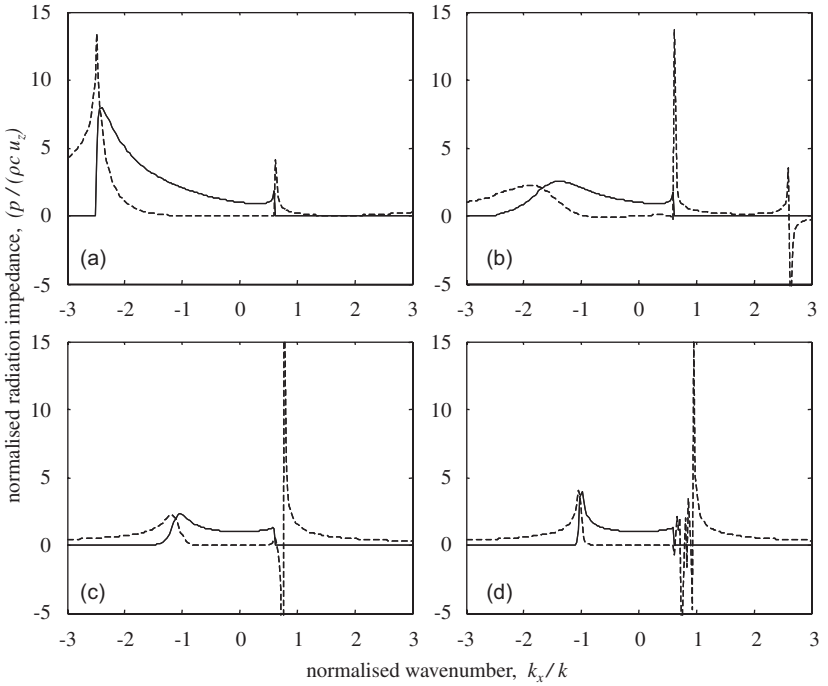

Fig. 2. Radiation impedance as a function of k_x and boundary layer thickness with $M_0 = 0.6$ and $k_y = 0$: (a) $\delta/\lambda = 0.01$, (b) $\delta/\lambda = 0.1$, (c) $\delta/\lambda = 1.0$, (d) $\delta/\lambda = 10$. Real part (—), imaginary part (- - - -).

spacing gives rise to a spatially periodic solution, with a period $L = 2\pi/\Delta k_x$ that is used to non-dimensionalise distances in each figure; for the data presented here $L = 1482\,\lambda$. The solution obtained from the inverse DFT is obtained at a set of 8192 locations uniformly spaced throughout the spatial domain.

Fig. 3 shows the pressure field generated by a 2D line source as a function of distance from the source, for three flow conditions: for zero flow, for a Mach 0.2 flow with a thin boundary layer ($\delta/\lambda = 0.001$), and for a Mach 0.2 flow with a thick boundary layer ($\delta/\lambda = 1.0$).

The zero flow case shows symmetry in the upstream and downstream directions and the expected 3 dB reduction in level, due to cylindrical spreading, for each doubling of distance. At large distances from the source the sound field decays more rapidly because of a small linear attenuation coefficient that is included in the model to control the magnitude of peaks in the radiation impedance, thus making the Fourier transforms better behaved. The attenuation was included in the model by specifying a complex speed of sound that, for the sign conventions of the theory used here and for the results presented, had a positive imaginary part equal to 0.1% of the absolute value of c_0.

With flow and with a thin boundary layer, Fig. 3(b), the level upstream is higher than the level downstream because of the effect of convective amplification. The ripple on the data is a numerical artefact that occurs because the flow means that the Fourier transform is not symmetric (in particular the value of the integrand at $k_x/k = -3$ is different from the value at $k_x/k = +3$) giving rise to a 'leakage' effect [3].

For the thick boundary layer, Fig. 3(c), the level falls off rapidly upstream because of the refractive effect of the boundary layer [4], whereas the level downstream is enhanced by channelling of the sound in the boundary layer.

3.3. Pressure field at the wall for a 3D point source

For the 3D solutions presented here, 2048×2048 point transforms were used in the evaluation of Eq. (5), with the same wavenumber ranges as for the 2D case. Figs. 4–6 show the pressure fields generated by a 3D point source for zero flow, for a Mach 0.3 flow with a thin boundary layer and a for a Mach 0.3 flow with a thick boundary layer. Each case is shown both as a contour plot on the x–y plane at $z = 0$ and as a graph of level versus distance upstream and downstream of the source along the line $y = 0$.

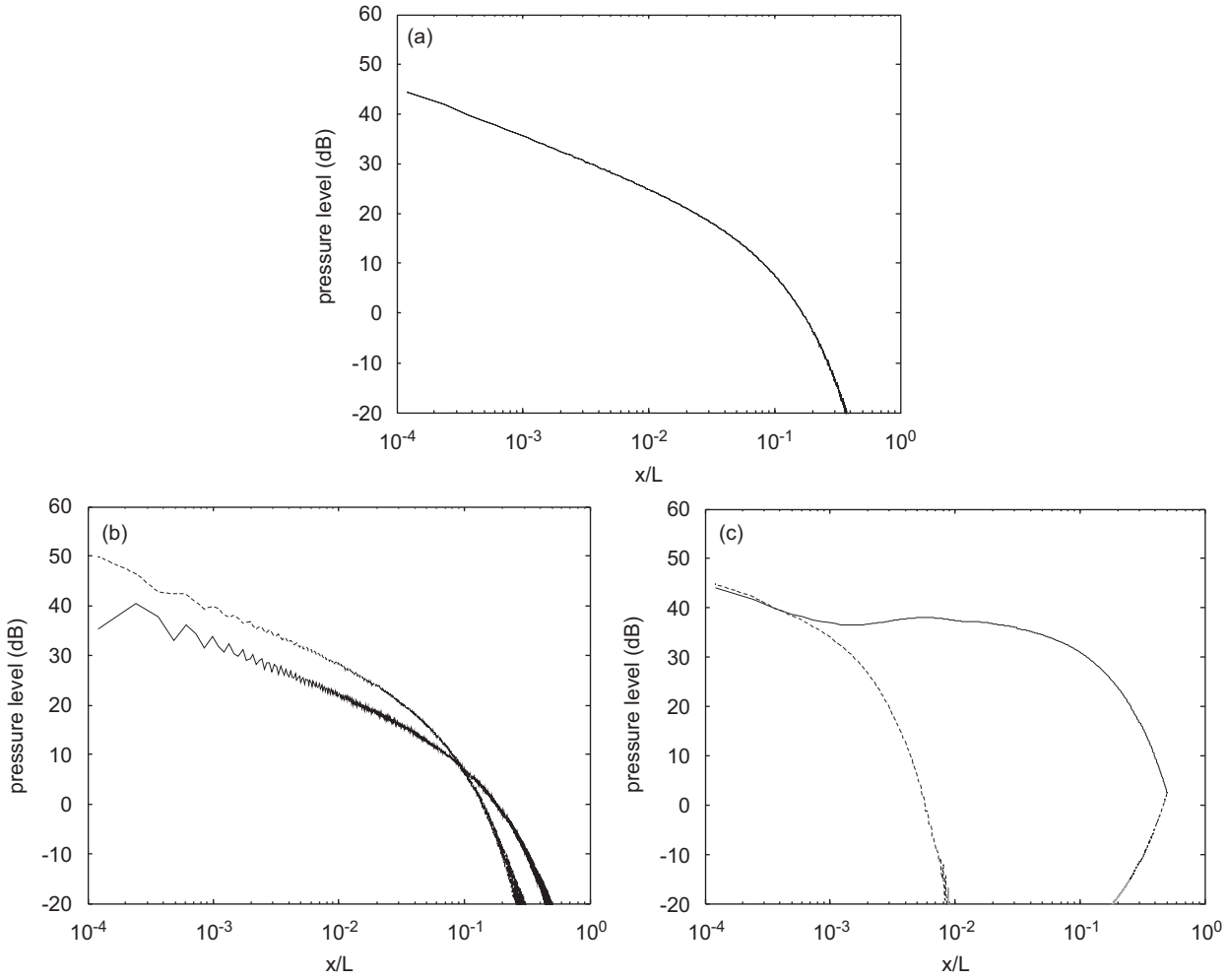

Fig. 3. Sound field upstream (----) and downstream (—) of a 2D source with various flow conditions: (a) Zero flow showing identical upstream and downstream pressures; (b) $M_0 = 0.2$, $\delta/\lambda = 0.001$; (c) $M_0 = 0.2$, $\delta/\lambda = 1.0$.

The zero flow case shows the expected features of a spherically spreading sound field, with a reduction in level of 6 dB for each doubling of distance. As for the 2D case, the rate of decay at large distances from the source increases because of damping in the model. Because the Fourier transform size is reduced, the physical scale is reduced by a factor of four compared with the 2D plots.

The plots with flow show the combined effects of convective amplification, which dominates in the case of a thin boundary layer, and upstream refraction away from the surface and downstream channelling near the surface, which occur with a thicker boundary layer. The shape of the contour plot in Fig. 6(a) may be of particular interest for a flow measuring device because the shape of the upstream shadow region could be of value in determining the flow direction.

4. Flow measurement using apparent convected phase velocity

4.1. Measurement of mean velocity in pipe flow

Ultrasonic flow measurement for fluid flowing in pipes is a well-established technique, which is generally based on the concept of a one-dimensional (1D) model of the convected phase velocity of sound propagation in a moving medium [1,2]. For a plane wave mode propagating in a rigid walled duct carrying a uniform flow,

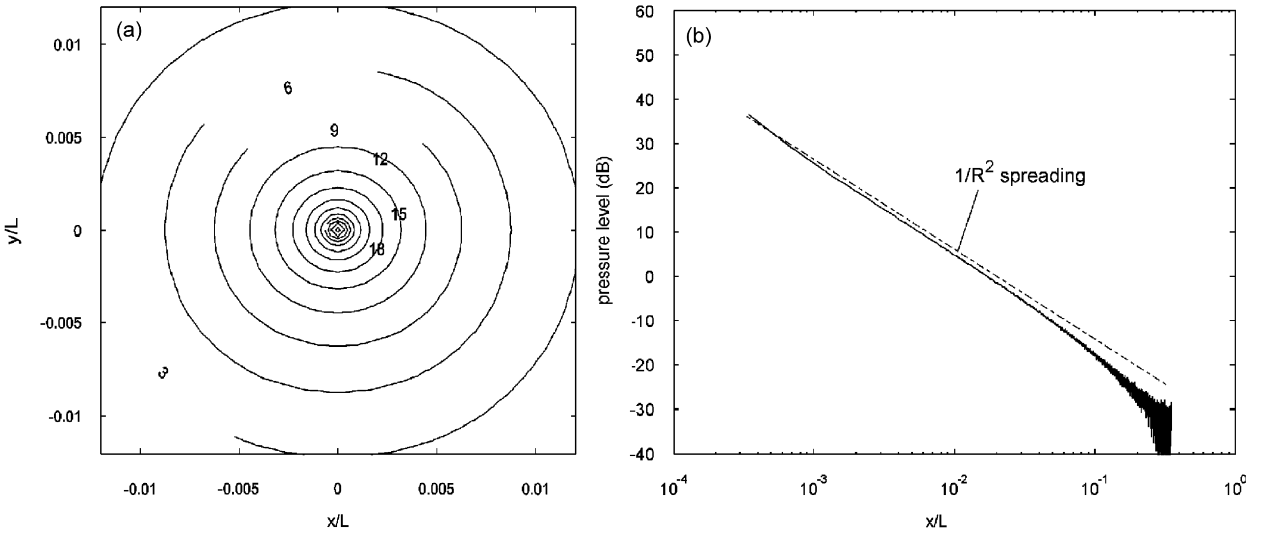

Fig. 4. Sound field around a 3D source centred at $x = 0$, $y = 0$; no flow: (a) contours of sound pressure level at $z = 0$, (b) Sound pressure level along the line $y = 0$.

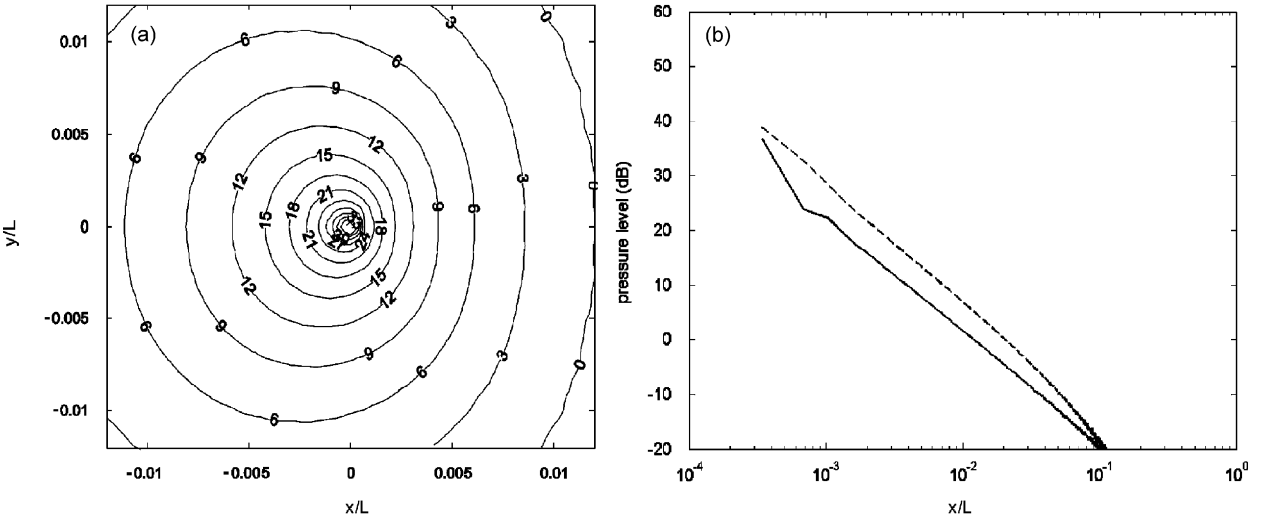

Fig. 5. Sound field around a 3D source centred at $x = 0$, $y = 0$; $M_0 = 0.3$ and $\delta/\lambda = 0.001$: (a) contours of sound pressure level at $z = 0$, (b) sound pressure level along the line $y = 0$; upstream (----) and downstream (—).

the phase velocity is $c_0(1 + M_0)$ in the downstream direction and $c_0(1-M_0)$ in the upstream direction. Here, c_0 is the speed of sound in stationary fluid and M_0 is the Mach number of the flow relative to this sound speed.

Instruments for measuring flow in a pipe commonly take a measurement of both upstream and downstream flight times, t_u and t_d, using two transducers separated by a distance l in the streamwise direction, so that the transducers act alternately as a source and then as a receiver. The Mach number of the flow and the speed of sound of the fluid may then be found by solving the following simultaneous equations:

$$\frac{l}{t_u} = c_0(1 - M_0), \tag{6a}$$

$$\frac{l}{t_d} = c_0(1 + M_0). \tag{6b}$$

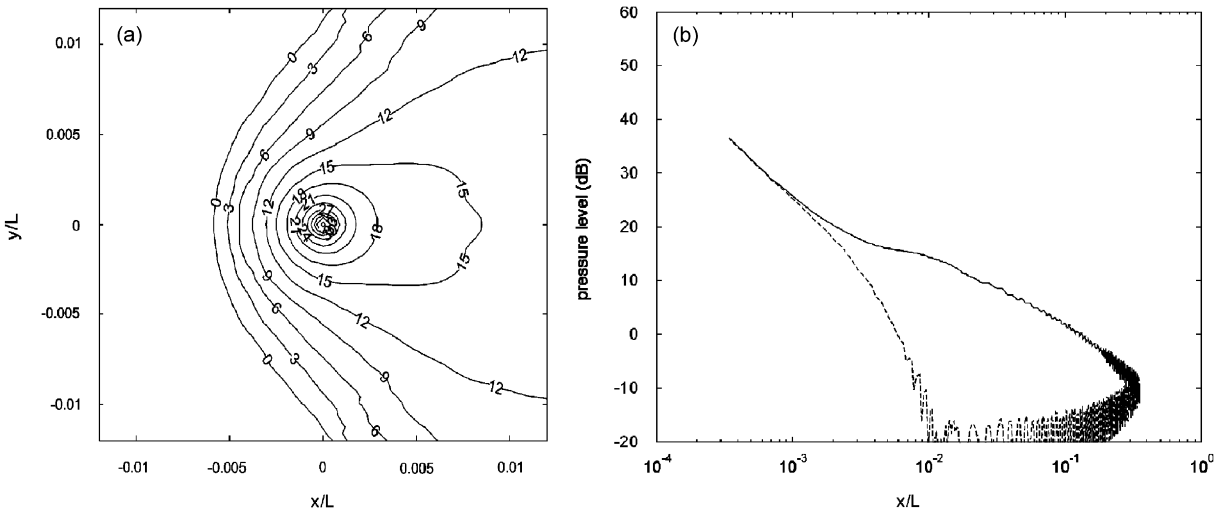

Fig. 6. Sound field around a 3D source centred at $x = 0$, $y = 0$; $M_0 = 0.3$ and $\delta/\lambda = 1.0$: (a) Contours of sound pressure level at $z = 0$, (b) Sound pressure level along the line $y = 0$; upstream (- - - -) and downstream (—).

Solving these equations for the flow Mach number gives

$$M_0 = \frac{l(t_u - t_d)}{2t_d t_u c_0} = \frac{l}{2c_0}\left(\frac{1}{t_u} - \frac{1}{t_d}\right). \tag{7}$$

Eq. (7) shows that the measurement of flow Mach number is dependant on the difference between the upstream and downstream times of flight, and one advantage of the dual measurement is that time delays inside the transducers or the electronics of the instrument cancel because of reciprocity; this makes the measurement technique far more robust. A second advantage of the dual measurement is that Eqs. (6a) and (6b) may also be solved to give the speed of sound c_0.

4.2. Measurement of free-stream velocity and boundary layer parameters

For transducers flush mounted under a boundary layer the upstream noise shadow effects described in the previous section mean that in practice only a downstream measurement of time of flight, t_d, can be made, and an independent measure of c_0 is required so that Eq. (6b) may be used to determine the apparent Mach number of the flow.

In terms of the complex pressure field downstream of the source at the wall, $p(x, 0, 0)$, predicted by a continuous wave model for a source of angular frequency ω, the propagation time from source to receiver is given by

$$t_d = \frac{1}{\omega}\int_l \frac{\mathrm{d}}{\mathrm{d}x}(\arg(p(x,0,0)))\,\mathrm{d}x. \tag{8}$$

For the discretised numerical solutions described in Section 3, comprising a set of points x_i, with the source and receiver defined to be at x_0 and x_n, respectively, the total phase change between source and receiver is approximated by the cumulative sum over the phase change between adjacent points. This approximation relies on the phase change between adjacent points being much less than π radians. Thus, the propagation time from the source point to the receiver point is given by

$$t_d(x_n) = \frac{1}{\omega}\sum_{i=0}^{n-1}(\arg(p(x_{i+1})) - \arg(p(x_i))) = \frac{1}{\omega}\sum_{i=0}^{n-1}\arg\left(\frac{p(x_{i+1})}{p(x_i)}\right). \tag{9}$$

The average phase velocity measured to this receiver location, expressed as a Mach number $M_d(x_n)$, is then calculated from

$$M_d(x_n) = \frac{(x_n - x_0)}{t_d(x_n)c_0}. \tag{10}$$

This is called the propagation Mach number in what follows.

4.3. Phase velocity downstream of a 2D line source: thin boundary layer

Figs. 7–9 illustrate this process for a zero flow case and for a Mach 0.3 flow with a thin boundary layer ($\delta/\lambda = 0.001$). The plots show the phase variation in both the upstream and downstream directions, with the upstream case being calculated using similar algorithms.

Fig. 7 shows the local phase at a series of points in a small region around a line source at $x/L = 0$, for the two cases. It is important to have many field points per wavelength so that there is no loss of phase information due to aliasing of the discretised spatial field. The cumulative sum of the phase change between points, the summation in (9), is plotted as a function of distance from the source in Fig. 8. The effective propagation Mach number between the source and each upstream and downstream field point is then plotted in Fig. 9.

When a mean flow of Mach number $M_0 = 0.3$ is applied, Figs. 7(b) and 9(b), it can be seen in that the rate of change of phase with distance is reduced in the downstream direction and increased in the upstream direction compared with the zero flow results in 7(a) and 9(a).

In the upstream direction, with flow, the rate of change of phase with distance is constant out to $x/L = -0.25$, but the graph then changes slope. This is due to the growing influence of image sources upstream as x/L takes larger negative values, as shown in Fig. 3(c), with energy from the primary source being refracted away from the surface. This illustrates a difficulty with upstream 'measurement' in the mathematical model that is analogous to the difficulty of upstream measurement in an experiment; in both cases the reduced level at the wall of the wave propagating upstream means that it is dominated by background noise.

The average propagation Mach number of sound as a function of distance downstream of the source is shown in Fig. 9. Close to the source there is a near field effect that perturbs the 'measurement', but the propagation Mach number quickly converges to the expected values, $(1 + M_0)$ downstream and $(1 - M_0)$ upstream. In the upstream direction with $M_0 = 0.3$ the 'measurement' gives a correct value out to a distance of approximately $x/L = -0.25$ but then diverges for the reasons noted above.

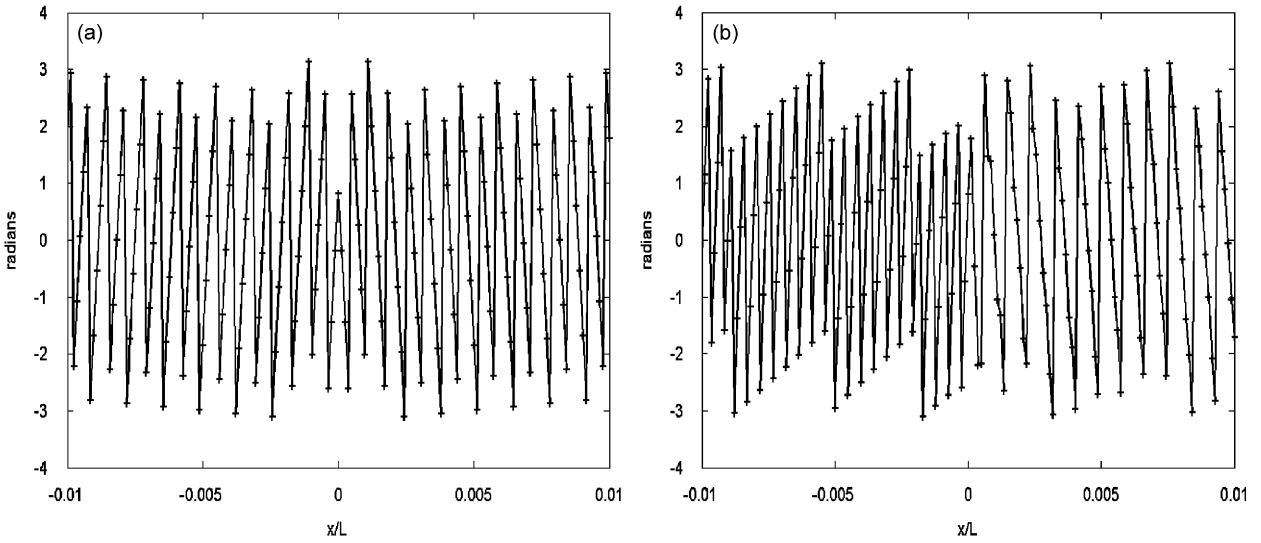

Fig. 7. Phase at field points, marked +, in the neighbourhood of a 2D line source for $\delta/\lambda = 0.001$: (a) $M_0 = 0$; (b) $M_0 = 0.3$.

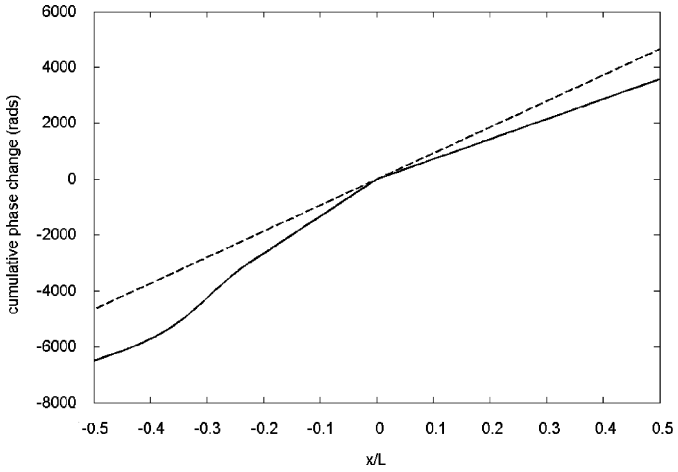

Fig. 8. Cumulative phase variation integrated upstream and downstream from $x = 0$ to $x = \pm L/2$: $M_0 = 0$ (----); $M_0 = 0.3$ and $\delta/\lambda = 0.001$ (—).

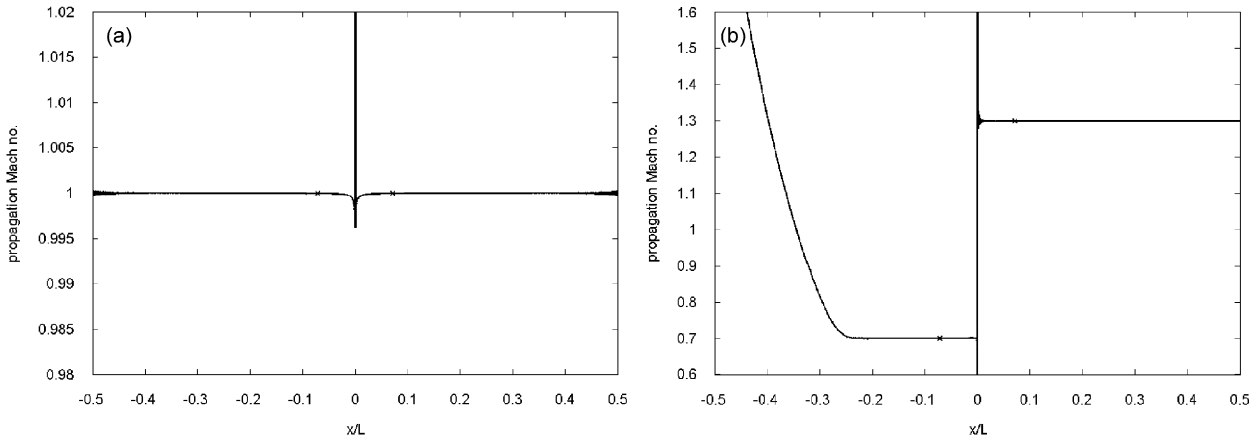

Fig. 9. Calculated propagation Mach number as a function of distance from the source: (a) $M_0 = 0$; (b) $M_0 = 0.3$, $\delta/\lambda = 0.001$.

In later sections, the effects of finite boundary layer thickness and of boundary layer profile on the excess downstream propagation Mach number, $M_e = (M_d - 1)$, will be considered. Figs. 9(a) and 9(b) show a cross at $x/L = 0.07$, which marks a point where all 'flow measurements' from the model will be made.

4.4. Phase velocity downstream of a 3D point source

The previous section showed that a 2D model gives the expected change in downstream propagation Mach number when there is a thin boundary layer. The present section considers a 3D geometry, to show firstly that the downstream result is the same as for 2D propagation, and then to demonstrate the effect of propagation transverse to the flow direction. The flow considered is again $M_0 = 0.3$ with $\delta/\lambda = 0.001$; the sound pressure level distribution around the source for this case was shown in Fig. 5.

Some care is needed in comparisons with the 2D model as an 8192 point transform was used to generate those results, whereas in the 3D problem a 2048×2048 double Fourier transform has been used. The discretisation rate was the same in each case, but the domain size L was reduced by a factor of four in the 3D problem. This means that plots versus x/L are scaled differently by this factor.

Fig. 10 shows the cumulative phase plot upstream and downstream of a point source located at (0,0), and comparison with Fig. 8 shows that the rate of change of phase with distance is identical in the

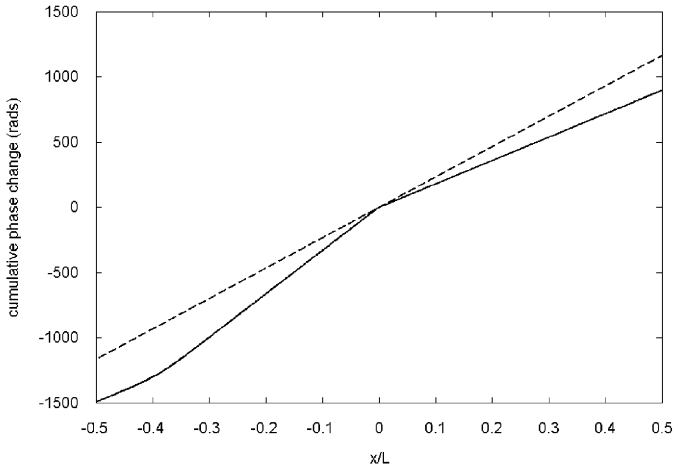

Fig. 10. Cumulative phase variation integrated upstream and downstream of a 3D point source at $x = 0$ to $x = \pm L/2$: zero flow (----); $M_0 = 0.3$, $\delta/\lambda = 0.001$ (—).

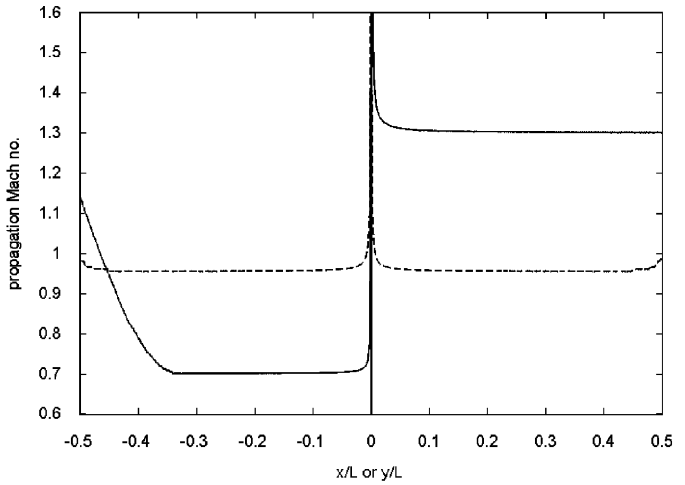

Fig. 11. Calculated propagation Mach number versus distance from a 3D source located at ($x = 0$, $y = 0$), $M_0 = 0.3$, $\delta/\lambda = 0.001$: upstream and downstream propagation, $y = 0$ (—); lateral propagation, $x = 0$ (----).

two problems, when account is taken of the scaling factor. The propagation Mach number directly upstream and downstream of the 3D source is shown in Fig. 11, and comparison with Fig. 9 shows that 'measurement' converges to the same result as the 2D case $(1 + M_0)$ downstream and $(1 - M_0)$ upstream. This result could have been anticipated since the waves propagating parallel to $y = 0$ in the 3D model have, by definition, a transverse wavenumber of $k_y = 0$ as is the case in the 2D model. The main difference between the 2D and 3D results is that the rate of convergence is affected by the factor of four change in length scale.

4.5. Phase velocity transverse to the flow direction

Fig. 11 also shows the result of measuring propagation Mach number along the line $x = 0$ which lies transverse to the flow. It might be thought initially that a value of $M_d = 1.0$ should be observed along this trajectory, but consideration of Fig. 12(a) shows why this is not the case. Sound arriving at the receiver may be considered to have propagated at Mach 1 along the path marked 1.0, and to be simultaneously convected

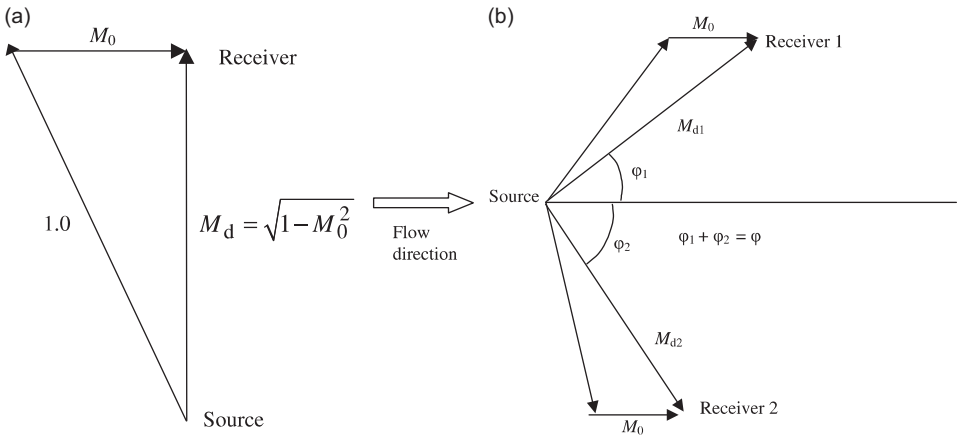

Fig. 12. Mach number vector diagrams: (a) calculation for a receiver on $x = 0$; (b) calculation of flow direction using a source and two receivers.

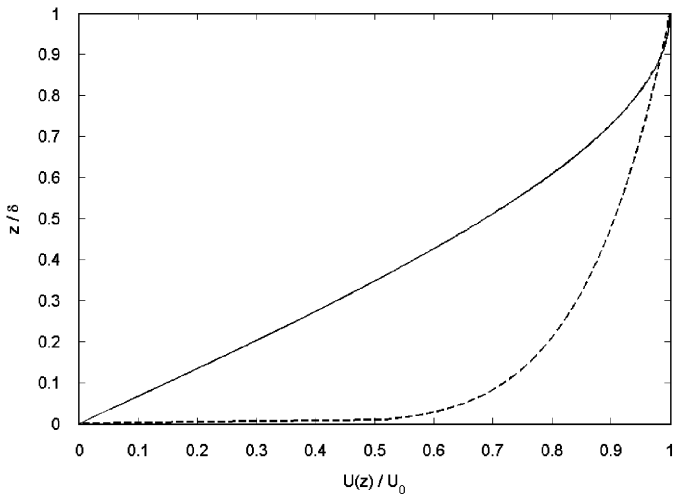

Fig. 13. Cubic (—) and 1/7th power law (- - - -) mean flow boundary layer profiles.

downstream at Mach number M_0 so that $M_d = \sqrt{1 - M_0^2}$; when $M_0 = 0.3$ a propagation Mach of $M_d = 0.954$ is expected, a figure that agrees well with the prediction in Fig. 11.

It is clear from this discussion that in principle a measurement of propagation Mach numbers using a source and two receiver locations separated by an angle φ may be used to calculate both the free-stream flow Mach number and the angle of the flow relative to the orientation of the three transducers. The situation is shown in the diagram in Fig. 12(b); measurements of M_{d1} and M_{d2} would allow M_0, φ_1 and φ_2 to be calculated.

4.6. Parameter study using the 2D model with flow

The 2D and 3D models have been shown to give the same result for downstream propagation at $\delta/\lambda = 0.001$, and this justifies the use of the 2D acoustic model to study the variation of propagation speed with flow Mach number, boundary layer thickness and boundary layer profile. Two boundary layer profiles

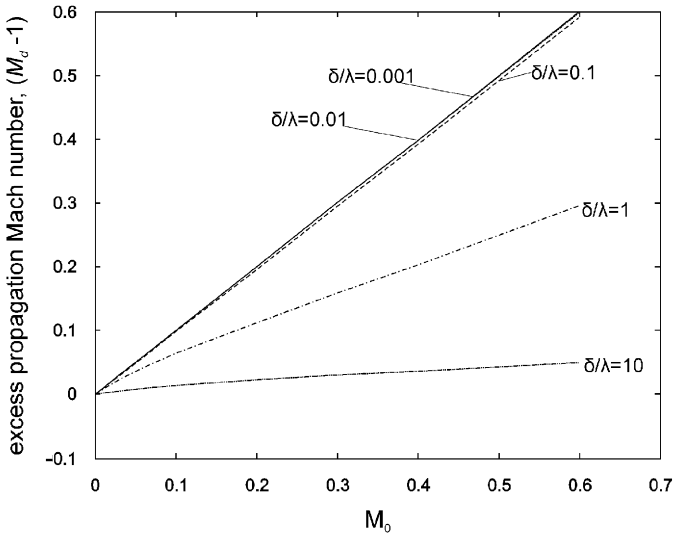

Fig. 14. Variation of excess propagation Mach number, (M_d−1), with free-stream Mach number and boundary layer thickness for a cubic power law boundary layer profile.

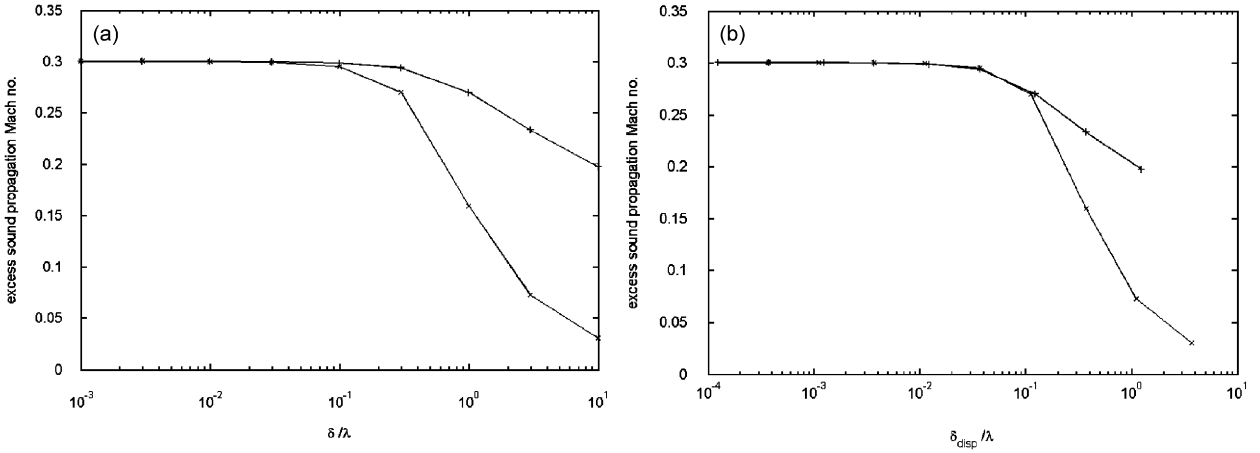

Fig. 15. Variation of excess propagation speed for cubic (+) and 1/7th power law (x) profiles as a function of: (a) boundary layer thickness δ, (b) displacement thickness δ_1. $M_0 = 0.3$.

are considered, a cubic profile which is representative of a laminar boundary layer, and a 1/7th power law profile that is representative of a turbulent boundary layer. The profile shapes are defined in Eq. (11) and plotted in Fig. 13:

$$U_{\mathrm{cub}}(z) = \frac{U_0}{2}\left(\frac{3z}{\delta} - \frac{z^3}{\delta^3}\right),$$
$$U_{1/7}(z) = U_0\left(\frac{z}{\delta}\right)^{1/7}. \tag{11}$$

Fig. 14 shows, for a flow with a cubic boundary layer profile, the dependence of excess propagation Mach number M_e on the free-stream Mach number M_0 and the non-dimensional boundary layer thickness δ/λ. With a thin boundary layer, $\delta/\lambda < 0.01$, it can be seen that the predictions fall on the line expected for uniform flow,

$M_e = M_0$. As the boundary layer grows in thickness beyond $\delta/\lambda = 0.1$ there is a strong variation of excess propagation Mach with boundary layer thickness.

A section through this plot for a fixed free-stream flow of $M_0 = 0.3$ is given in Fig. 15(a), giving the variation of M_e with boundary layer thickness δ at this Mach number. In this figure, data are shown for both the cubic profile and the 1/7th power law profile, showing significantly different results for the two types of boundary layer. The data of Fig. 15(a) are re-plotted versus boundary layer displacement thickness, δ_1, in Fig. 15(b). By integration of the boundary layer profiles defined in (11) it is easy to show that $\delta_1 = 0.125\,\delta$ for a 1/7th power law profile and $\delta_1 = 0.375\,\delta$ for a cubic profile, so that for a given value of δ there is a factor of 3 difference in the value of δ_1 between the two profiles. Removing this factor collapses the two data sets for $\delta_1/\lambda < 0.1$, indicating that the variation in M_e is dependant on this parameter. Plotting the data versus other boundary layer parameters, such as momentum thickness or kinetic energy thickness, for which the scaling factor between for the two boundary layer profiles is 1.43 and 1.23, respectively, would produce a less satisfactory collapse.

The similarity of the two curves in Fig. 15(b) for boundary layers satisfying $\delta_1/\lambda < 0.1$ means that in principle, by measuring the phase velocity at two suitable frequencies, it is possible to determine both the free-stream velocity and the boundary layer displacement thickness. The two frequencies f_1 and f_2 should ideally have wavelengths satisfying $\delta_1/\lambda < 0.01$ and $\delta_1/\lambda \sim 0.1$, i.e. $f_1 < (c_0/100\delta_1)$ and $f_2 \approx (c_0/10\delta_1)$. A practical measuring device could use a broadband signal containing a range of frequencies to cover a range of boundary layer thicknesses, assuming that such a broadband transducer could be built.

5. Experimental validation

This section describes an experiment that was undertaken as a consultancy project to test the concept of measuring mean flow over a surface using ultrasound. The original study was focussed on measurement of the free-stream flow, rather than the boundary layer parameters, so that no independent method of measuring boundary layer thickness was available. The project was carried out collaboratively between ISVR and Gill Electronic R&D and was funded by DERA (now QinetiQ).

5.1. Test apparatus

Fig. 16 shows a test fixture designed to produce a boundary layer of variable thickness over a flat plate containing the flow transducer; the fixture could be angled downwards vary the angle of attack into the flow,

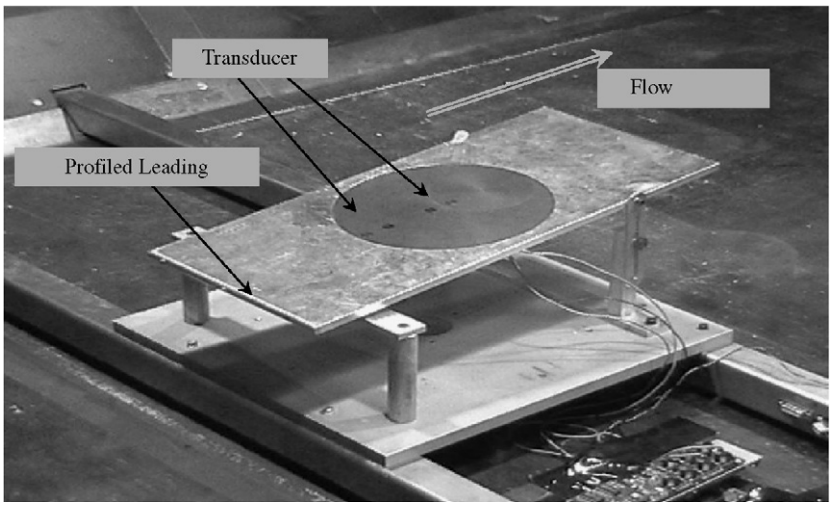

Fig. 16. Test arrangement showing the ultrasonic transducers mounted in rotatable housings in the flat plate fixture.

and the leading edge of the plate could be either square or profiled to alter the initial growth of the boundary layer.

The test equipment for measuring phase speed was based on development hardware for standard Gill free-field anemometers, with adaptations for measurements at a wall, and used a pulse of ultrasound with a primary frequency of approximately 180 kHz. Details of the measurement method used in the instrument are beyond the scope of this paper.

Each transducer comprised a cylindrical piezo-electric crystal with an impedance matching layer. The radius of the transducer face, a, was approximately 2.5 mm, so that $ka \approx 8$ at the operating frequency. In their usual application, the transducers are required to radiate a narrow beam along their cylindrical axis and this large ka value is advantageous. In the wall mounted application however the transducers are required to radiate laterally and so the transducers were each mounted under a cap with a 1 mm radius hole, thus reducing the effective source size to $ka = 3.2$, below the value of $ka = 3.83$ at which side lobes are expected to occur [7]. The transducers were mounted in rotatable housings so that their spacing, nominally 0.104 m for data presented here, and orientation relative to the flow could be varied.

5.2. Downstream propagation with source and receiver aligned in the flow

5.2.1. Measured data

The data presented in this section are for the receiver positioned downstream of the source. Measurements were made with flow velocities of 0–45 in 5 m/s steps with the plate configured as follows:

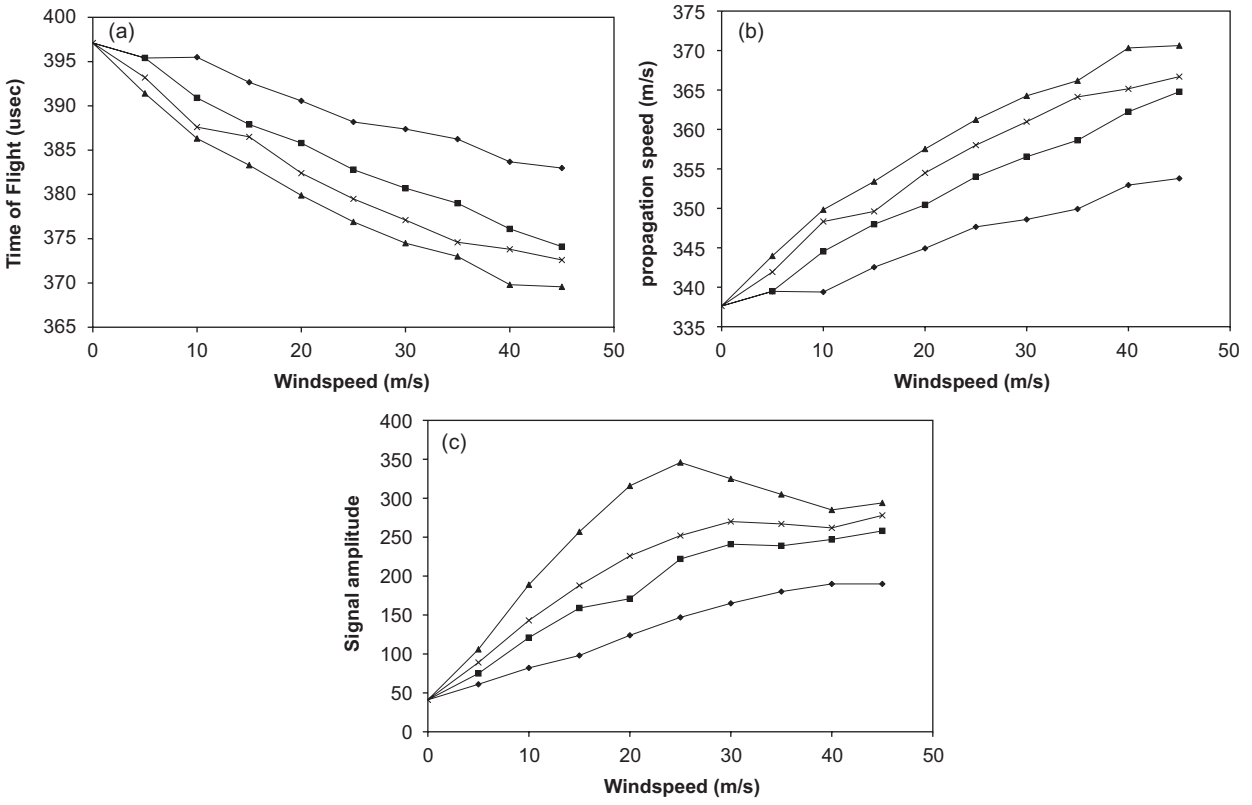

Fig. 17. Experimental data from wind tunnel tests: (a) time of flight as a function of tunnel wind speed and angle of incidence. (b) Apparent propagation speed derived from time of flight data. (c) Amplitude of downstream signal amplitude for square and profiled leading edges —◆— 0° square leading edge, —■— 0° profiled leading edge, — × — −6° square leading edge, —▲— −6° profiled leading edge.

- 0° angle of attack, square leading edge,
- 0° angle of attack, semi-circular leading edge,
- -6° angle of attack, square leading edge,
- -6° angle of attack, semi-circular leading edge.

The raw test data, namely the measured time of flight in μs and the amplitude of the downstream signal, are shown in Fig. 17(a) and (b), and Fig. 17(c) shows the propagation speed deduced from the data. The data have been corrected for minor temperature variations during the course of the experiments.

It may be expected that applying a negative angle of attack or using a round leading edge would reduce the thickness of the boundary layer over the transducer, and hence increase the pulse propagation speed. This effect is clearly seen in the data, with the round leading edge at -6° angle of attack giving the highest propagation speed, and the square leading edge at 0° angle of attack giving the lowest propagation speed.

With respect to the receiver amplitude information shown in Fig. 17(b), the increase in level with wind speed is explained by the channelling effect noted in Section 3. The effect is partially limited by the fact that the boundary layer gets thinner as the velocity increases. Another contributory factor is that the directivity of the transducer is altered, with the main directivity lobe being progressively directed downstream as the flow rate increases [4].

5.2.2. *Comparison of the test rig measurements and the prediction model for downstream propagation*

To make quantitative comparisons between the test measurements and the prediction model it is necessary to determine the mean boundary layer thickness between the source and receiver transducer locations. The only configuration for which the boundary layer thickness can reasonably be estimated from first principles is the test with the profiled leading edge and 0° angle of attack. The thickness of a laminar boundary layer on a flat plate may be calculated from the Reynolds number based on distance from the leading edge using the formula:

$$\frac{\delta_{99}}{x} = 4.91\,\mathrm{Re}_x^{-0.5}, \tag{12}$$

where $\mathrm{Re}_x = (M_0 c_0 x/\nu)$ and ν is the kinematic viscosity. The boundary layer thickness to wavelength ratio at the mid point of the transducer is plotted as a function of flow velocity in Fig. 18. The boundary layer is approximately 1.4 wavelengths thick at 10 m/s and half that at 45 m/s. No account will be taken of the changing boundary layer thickness over the distance between the transducers.

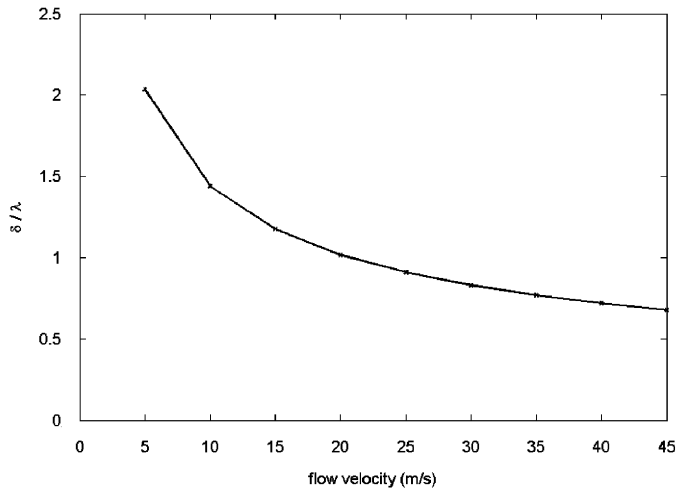

Fig. 18. Estimated boundary layer thickness at the mid transducer location for the test rig at 0° angle of incidence and with a profiled leading edge.

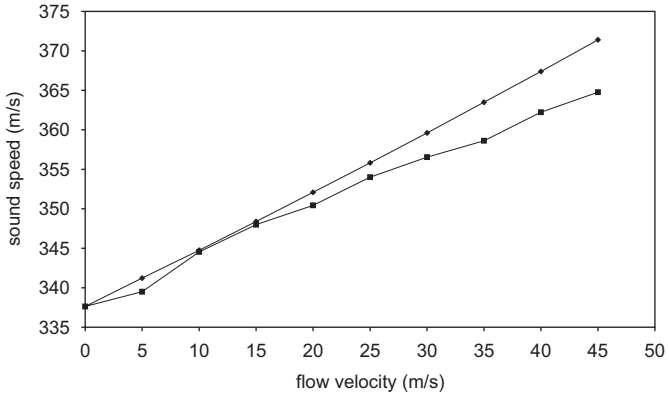

Fig. 19. Comparison of predicted and measured variation of convected wave speed as a function of wind tunnel flow velocity; receiver downstream of a $ka = 2.84$ source. —◆— predicted, —■— measured.

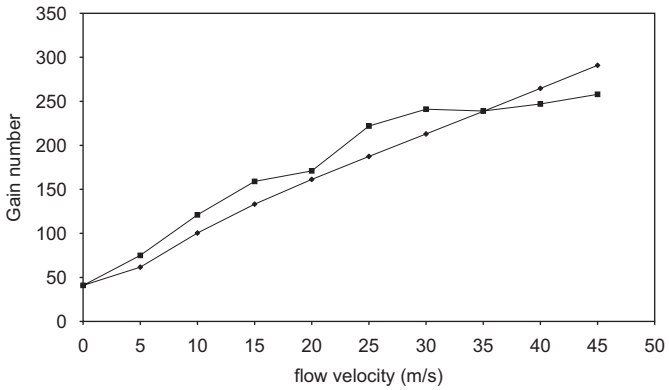

Fig. 20. Predicted and measured variation of gain number as a function of wind tunnel flow velocity; receiver downstream of source of a $ka = 2.84$ source. —◆— predicted, —■— measured.

Using this estimate of boundary layer thickness the mathematical model may be used to simulate the appropriate data from Fig. 17. The source ka value used in the predictions was 2.84, compared with the nominal value of $ka = 3.3$ for the actual source.

The predicted and measured convected wave speed data are shown in Fig. 19, and the predicted and measured signal amplitude is given in Fig. 20. In both cases the predictions have been scaled to give the correct measured value at zero flow velocity; for the velocity calculation this was a correction to account for the time delay associated with transmission through the transducers, for the amplitude this was effectively a calibration of the source.

For both the velocity data and the amplitude data the model agrees fairly well with the measurements, predicting changes to within 15% accuracy. This agreement is good considering some of the approximations which are included in the model and in the measurements, for example:

- The assumption of a constant boundary layer thickness between source and receiver.
- The relatively crude estimate of boundary layer thickness, especially considering the thick leading edge of the plate.
- The method of approximating the actual source directivity.
- The accuracy of the time of flight and pulse amplitude measurements which, although dominated by the 180 kHz carrier frequency, may be affected by the dispersive effects.

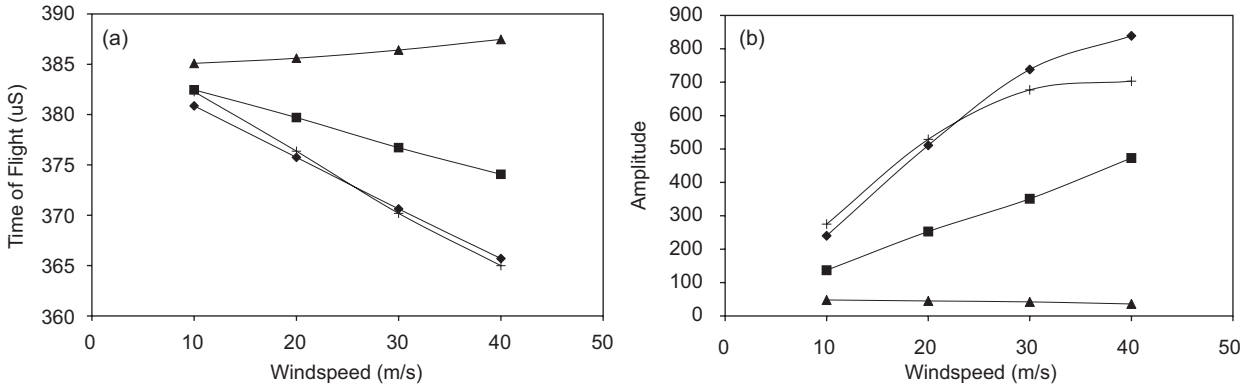

Fig. 21. Data for sound propagation at various angles to the direction of flow: —+— 0° (downstream), —◆— 30°, —■— 60°, —▲— 90° (cross-flow), (a) time of flight; (b) signal amplitude.

5.3. *Propagation transverse to the flow*

The nested rotatable housings, just visible in Fig. 16, were used to vary the angle of the transducer pair in the flow. Tests were only performed with a -6° angle of attack on the plate so that quantitative comparisons with the mathematical model are difficult, but qualitative comparisons can be made.

Measured time of flight data are presented in Fig. 21(a) and the corresponding amplitude data are shown in Fig. 21(b). As predicted in Section 4.2, the time of flight is generally lowest for downstream propagation, 0° rotation, and is highest when the transducers are rotated to an angle of 90° to the flow. For the latter case the time of flight increases slightly with increasing flow velocity, as predicted in Section 4.2.

The trends in the amplitude data are also consistent with the findings from the mathematical model; the amplitude is greatest in the downstream direction and there is a reduction in amplitude for propagation at 90° to the flow.

6. Conclusions

A model of sound radiation into a shear flow has been used to predict the phase velocity of sound convected between a source and a downstream receiver. This has been used to demonstrate the principle of a flow-measuring device.

The model shows that an instrument working at a frequency where the boundary layer is thin on the wavelength scale would measure the free-stream Mach number of the flow. For boundary layers greater than one hundredth of a wavelength thick the phase velocity is reduced. It is shown that this dispersive effect is potentially useful as a means of determining some parameters of the boundary layer. Measuring at two appropriate frequencies could give free-stream velocity and boundary layer displacement thickness. Using more frequencies could potentially give further information about the boundary layer profile. The variation of amplitude and/or convected phase speed with angle downstream is also shown to be potentially useful for determining the direction of the local flow vector.

The model has been validated by a preliminary experiment using a prototype sensor in a wind tunnel. The sensor displayed a fairly linear relationship between convected speed of sound and actual flow velocity for free-stream flow velocities up to 45 m/s, Mach 0.12. The prediction model suggests that this linear relationship continues to higher subsonic Mach numbers.

The relationship between convected speed of sound and boundary layer thickness has been confirmed qualitatively in the experiment by varying the angle of attack and the leading edge of the plate to change the flow conditions over the transducers. For the one test case where it was possible to predict the boundary layer thickness with reasonable accuracy from first principles, with $0.0875 < \delta_1/\lambda < 0.25$ depending on flow velocity, the measured variation of convected speed of sound agreed well with the predictions of the model. For sound

propagation transverse to the flow the variation of both the convected speed of sound and the amplitude agreed qualitatively with the predictions of the model.

Acknowledgements

The authors acknowledge the contribution of D. Greenwell, formerly of DERA (now Qinetiq) and now at Bristol University, who initiated and participated in the DERA funded project on which this paper is partly based. They also wish to thank Professor C.L. Morfey, Professor Emeritus at ISVR, who contributed to this work as academic supervisor to M.G. Smith during the course of the project and subsequent studies.

Appendix A. Governing equation for acoustic impedance

Use of Eq. (5) to calculate the sound field around the source requires the radiation impedance for outgoing waves propagating through the boundary layer, $Z_{\mathrm{rad}}(k_x, k_y)$; this Appendix derives the governing equation that has to be solved in order to calculate Z_{rad}. More details are given in Refs. [3,4], but the focus here is on a simplification of the problem which arises because the model is only required to predict the acoustic pressure at the wall, $z = 0$.

The starting point is the linearised inviscid momentum and continuity equations in vector notation. For small amplitude perturbations of the flow shown in Fig. 1, these are [5]

$$\rho_0\left(\overline{D}\mathbf{u} + (\mathbf{u}\cdot\nabla)\mathbf{U}\right) = -\nabla p, \tag{A.1}$$

$$\frac{1}{\rho_0 c_0^2}\overline{D}p = -\nabla\cdot\mathbf{u}. \tag{A.2}$$

Here, $\mathbf{U}$ is the mean velocity vector, $\mathbf{u}$ is the acoustic particle velocity vector with components (u_x, u_y, u_z), p is acoustic pressure, ρ_0 is the local fluid density (which will be assumed constant) and c_0 is the local speed of sound. $\overline{D}$ is the operator $(\partial/\partial t) + \mathbf{U}\cdot\nabla$, and subscript 0 denotes unperturbed values.

Fourier transforming these equations in the variables x, y and t leads to a set of simultaneous equations for the transformed acoustic variables u_x, u_y, u_z and p. The variables u_x and u_y may be eliminated, leading to the following coupled equations in u_z and p:

$$\frac{\partial u_z}{\partial z} = -\frac{1}{\rho_0\overline{D}}\left(\left(\frac{\overline{D}^2}{c_0^2} + k_x^2 + k_y^2\right)p + jk_x\rho_0 u_z\frac{\mathrm{d}U}{\mathrm{d}z}\right), \tag{A.3}$$

$$\frac{\partial p}{\partial z} = -\rho_0\overline{D}u_z. \tag{A.4}$$

In these transformed equations $\bar{D} = j(\omega - k_x U)$. Combining these equations to eliminate u_z leads directly to the second order differential equation derived by Pridmore-Brown [8].

The radiation impedance of the surface is given by the ratio of pressure and normal particle velocity in the fluid at $z = 0$ for an outward propagating wave, i.e.:

$$Z_{\mathrm{rad}} = Z(0) \quad \text{where} \quad Z(z) = \frac{p(z)}{u_z(z)}. \tag{A.5}$$

Differentiating Z with respect to the z-coordinate and substituting using (A.3) and (A.4) leads to the following equation for the variation of impedance through the parallel flow:

$$\frac{\mathrm{d}Z}{\mathrm{d}z} = \frac{1}{\rho_0}\left(\frac{\overline{D^2}}{c_0^2} + k_x^2 + k_y^2\right)Z^2 + jk_x\rho\frac{\mathrm{d}U}{\mathrm{d}z}Z - \rho_0\overline{D}. \tag{A.6}$$

In the region of uniform flow the impedance is constant so that $(dZ/dz) = 0$. From Eqs. (A.5) and (A.7) therefore, it may be seen that outside the boundary layer:

$$Z = \frac{-j\rho_0 \overline{D}}{k_z}, \tag{A.7}$$

where $k_z = \sqrt{(\omega - k_x U_0)^2/c_0^2 - k_x^2 - k_y^2}$.

Starting from this initial value and integrating Eq. (A.6) through the boundary layer gives the radiation impedance at the wall:

$$Z_{\mathrm{rad}}(k_x, k_y) = Z(k_x, k_y, 0). \tag{A.8}$$

By this method of solution the radiation impedance is obtained without the need to explicitly solve for the acoustic field variables p and u_z.

Eq. (A.6) is sometimes inconvenient because the dU/dz term may become infinite in some circumstances, for example for an assumed 1/7th power law turbulent boundary layer flow profile or for an infinitely thin shear layer. Refs. [3,4] discuss alternative equations that can be obtained by using the displacement impedance variable χ, the ratio of the acoustic pressure p and the particle displacement q, in place of Z. In a practical implementation of the integration through the boundary layer equations in both variables may be useful to avoid the numerical difficulties discussed in Refs. [3,4]. For example, in considering radiation into a turbulent boundary layer at a wavenumber at which a critical layer occurs, Z should be integrated from the edge of the boundary layer through the critical layer; χ is then calculated and used at the variable to integrate to the wall.

References

[1] V. Pagneux, B. Froelich, Influence of low Mach number shear flow on acoustic propagation in ducts, *Journal of Sound and Vibration* 346 (1) (2001) 137–155.
[2] Gill Instruments Ltd. web site ⟨http://www.gill.co.uk⟩.
[3] M.G. Smith, Sound Radiation from a Vibrating Surface Under a Boundary Layer, PhD Thesis, ISVR, University of Southampton, UK, 2004.
[4] M.G. Smith, C.L. Morfey, Directivity and sound power radiated by a source under a boundary layer, *AIAA Journal* 44 (11) (2006) 2630–2635.
[5] M.E. Goldstein, Unified approach to aerodynamic sound generation in the presence of solid boundaries, *Journal of the Acoustical Society of America* 56 (1974).
[6] Morse, Ingard, *Theoretical Acoustics* (1986).
[7] A.D. Pierce, *Acoustics, An Introduction to its Physical Principles and Applications*, Acoustical Society of America, New York, 1989.
[8] D.C. Pridmore-Brown, Sound propagating in a fluid flowing through an attenuating duct, *Journal of Fluid Mechanics* 4 (1958) 393–406.